Since January 2020 Elsevier has created a COVID-19 resource centre with free information in English and Mandarin on the novel coronavirus COVID-19. The COVID-19 resource centre is hosted on Elsevier Connect, the company's public news and information website.

Journal of Hazardous Materials 429 (2022) 127709

Contents lists available at ScienceDirect

Journal of Hazardous Materials

journal homepage: www.elsevier.com/locate/jhazmat

Efficacy and self-similarity of SARS-CoV-2 thermal decontamination

Te Faye Yap [a,1], Jason C. Hsu [b,1], Zhen Liu [a], Kempaiah Rayavara [b], Vivian Tat [b], Chien-Te K. Tseng [b,c], Daniel J. Preston [a,*]

[a] Department of Mechanical Engineering, George R. Brown School of Engineering, Rice University, 6100 Main St., Houston, TX 77005, USA
[b] Department of Microbiology and Immunology, University of Texas Medical Branch, 301 University Blvd., Galveston, TX 77555, USA
[c] Center for Biodefense and Emerging Diseases, Galveston National Laboratory, University of Texas Medical Branch, 301 University Blvd., Galveston, TX 77555, USA

HIGHLIGHTS

- Empirical data alone does not explain the thermal virus inactivation reaction.
- This work develops and validates a modeling framework based on reaction kinetics.
- The results reveal self-similar behavior during inactivation of coronaviruses.
- Heating surgical masks to 70 °C for 5 min inactivates > 99.9% of SARS-CoV-2.
- XPS, SEM, and contact angle show no physical or chemical degradation of the masks.

GRAPHICAL ABSTRACT

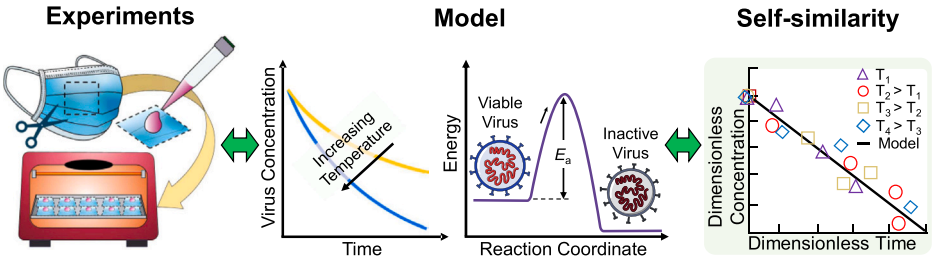

ARTICLE INFO

Editor: Dr. Danmeng Shuai

Keywords:
COVID-19
Dry heat decontamination
Personal protective equipment
Arrhenius equation
Reaction rate law

ABSTRACT

Dry heat decontamination has been shown to effectively inactivate viruses without compromising the integrity of delicate personal protective equipment (PPE), allowing safe reuse and helping to alleviate shortages of PPE that have arisen due to COVID-19. Unfortunately, current thermal decontamination guidelines rely on empirical data which are often sparse, limited to a specific virus, and unable to provide fundamental insight into the underlying inactivation reaction. In this work, we experimentally quantified dry heat decontamination of SARS-CoV-2 on disposable masks and validated a model that treats the inactivation reaction as thermal degradation of macromolecules. Furthermore, upon nondimensionalization, all of the experimental data collapse onto a unified curve, revealing that the thermally driven decontamination process exhibits self-similar behavior. Our results show that heating surgical masks to 70 °C for 5 min inactivates over 99.9% of SARS-CoV-2. We also characterized the chemical and physical properties of disposable masks after heat treatment and did not observe degradation. The model presented in this work enables extrapolation of results beyond specific temperatures to provide guidelines for safe PPE decontamination. The modeling framework and self-similar behavior are expected to extend to most viruses—including yet-unencountered novel viruses—while accounting for a range of environmental conditions.

1. Introduction

The COVID-19 pandemic has challenged the global healthcare system and exposed frontline healthcare workers to an unacceptable level of risk. The relatively high reproduction number of SARS-CoV-2 (Sanche et al., 2020; Zhu and Chen, 2020) has resulted in a surge in

* Corresponding author.
E-mail address: djp@rice.edu (D.J. Preston).
[1] Equal contribution

https://doi.org/10.1016/j.jhazmat.2021.127709
Received 8 September 2021; Received in revised form 1 November 2021; Accepted 2 November 2021
Available online 7 November 2021

hospitalization rates and, in turn, a shortage of personal protective equipment (PPE); in many instances, disposable masks had to be reused (Kolata, 2020; Rowan and Laffey, 2020). Despite the rollout of vaccines, PPE shortages may continue to occur in countries with a relatively low Human Development Index for years to come, and this risk is elevated by the rise of dangerous variants (Callaway, 2021; Mahase, 2021; Samarasekera, 2021). Various decontamination methods—including UV irradiation, steam sterilization, and chemical disinfectants—have been implemented, but these methods suffer from several drawbacks, namely: (i) UV irradiation only inactivates viruses that are illuminated and is ineffective within folds and crevices commonly present in fabric-based PPE (Cramer et al., 2020; Jinia et al., 2020; Raeiszadeh and Adeli, 2020); (ii) steam or moist heat sterilization relies on water vapor at high temperatures and pressures to sterilize equipment at a relative humidity of 100%, which can compromise the filtration efficiency of masks (Campos et al., 2020); and (iii) chemical disinfectants leave harmful chemical residues within the porous structures of some PPE and may degrade the material (Jinia et al., 2020; Viscusi et al., 2009).

Dry heat decontamination is performed at elevated temperatures, but at relative humidities less than 100%, by heating the air surrounding the equipment to be decontaminated. The high elevated temperatures applied during typical dry heat decontamination have been shown to degrade polymer-based PPE (Viscusi et al., 2007). However, when performed at lower elevated temperatures (albeit over longer periods of

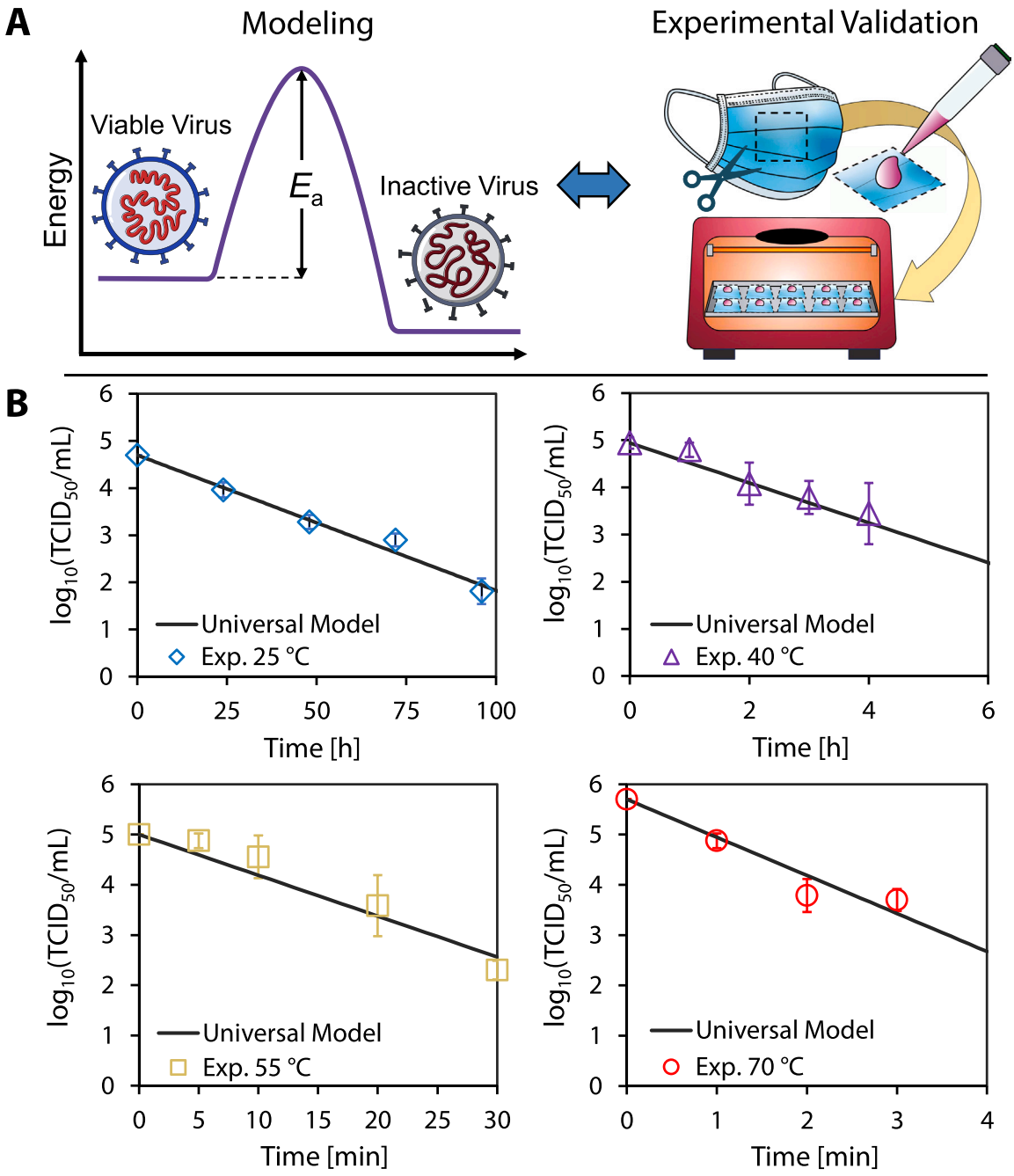

Fig. 1. Validation of model with experimental results. (A) The universal model combines the rate law and the Arrhenius equation to determine the activation energy required to inactivate a specific virus. Surgical mask samples were inoculated with SARS-CoV-2 and exposed to 25 °C, 40 °C, 55 °C, and 70 °C dry heat in an oven. (B) The samples were assayed at different times; the plots show the corresponding $\log_{10}$ viable virus concentration at each time point for a given temperature. Each experimental data point was assayed in triplicate, and error bars correspond to the standard deviation among the triplicate measurements. Our universal model based on the reaction kinetics was plotted, and exhibited close agreement with experimental data.

time), dry heat decontamination represents a promising alternative to other approaches and has been shown to effectively inactivate viruses while retaining the efficacy and integrity of disposable masks (Liao et al., 2020; Oh et al., 2020). Moreover, appliances for dry heat decontamination are attainable in most households (*e.g.*, home ovens or rice cookers). Oh et al. demonstrated the feasibility of dry heat decontamination of N95 respirators using a household electric cooker and found that the filtration performance and fit of the respirators were not compromised after 20 cycles of heat treatment (Oh et al., 2020). Other experiments on the thermal decontamination of SARS-CoV-2 have been performed on various surfaces across a range of temperatures, providing empirical guidelines for PPE decontamination (Campos et al., 2020; Chin et al., 2020; van Doremalen et al., 2020). These experimental results are promising, but they are often sparse, only reflect virus inactivation at specific temperatures, and do not provide a fundamental understanding of the effect of temperature on the rate of virus inactivation. On the other hand, analytical models which treat viruses as macromolecules undergoing thermal degradation have been used to describe the relationship between temperature and virus inactivation (Yap et al., 2020), but these models have not been validated with experimental results. A reliable model would reduce the number of experiments required to capture the thermal inactivation behavior of a specific virus while also providing comprehensive thermal decontamination guidelines. In this work, we experimentally quantified the thermal decontamination of surgical masks inoculated with SARS-CoV-2, and, using the results, we validated a model of the virus inactivation reaction that can predict the lifetime of SARS-CoV-2 as a continuous function of temperature (Fig. 1A).

2. Materials and methods

2.1. SARS-CoV-2 thermal inactivation experiments

We conducted dry heat decontamination experiments at 25 °C, 40 °C, 55 °C, and 70 °C at a relative humidity within the range of 48 – 55% in a biosafety cabinet. We chose 25 °C to correspond to standard ambient conditions. We chose 70 °C as our maximum temperature for three reasons: (i) it is the lowest setting in typical home ovens; (ii) it has been suggested as a dry heat decontamination temperature by the FDA; and (iii) 70 °C is a typical temperature used for pasteurization (Iijima et al., 2001; Islam and Johnston, 2006; Xiang et al., 2020; Zha et al., 2021). Surgical masks (Canuxi Disposable Face Masks, SKU 810484847) were cut into 5 cm by 5 cm samples and inoculated with SARS-CoV-2 virus stock. The samples were placed on an oven pan and heated in a home-use oven (Brentwood, TS-345R) at the specified decontamination temperatures. The countertop oven and stainless-steel oven pan were preheated to the desired inactivation temperature and monitored with a digital thermometer (Fisherbrand, 14–648–46). The temperature dial settings for the three temperatures tested in this study were measured and determined beforehand in a biosafety cabinet (BSC) at a BSL-2 laboratory in order to replicate potential experimental conditions in a low-risk environment. Then, either a 1 mL droplet of the low-titer virus culture (for the 25 °C, 40 °C, and 55 °C experiments) or a 100 μL droplet of the high-titer virus culture (for the 70 °C experiment) was pipetted onto the outer layer of each surgical mask sample and left at room temperature (~25 °C) while the oven was preheating. When the oven temperature stabilized within ± 3 °C of the desired temperature for 30 min, the oven pan was taken out and each inoculated mask sample was carefully transferred (taking approximately five seconds per mask sample) onto the oven pan with the viral inoculum side facing upwards and placed back inside the oven for dry heat treatment. Each mask piece was removed from the oven once the desired time point was attained and immediately soaked in 10 mL of 2% FBS-MEM virus transfer medium in a 50 mL conical centrifuge tube for at least 30 min to recover the virus.

After the 30 min elapsed, the recovered virus medium was titrated *via* a standard $TCID_{50}$ assay procedure (Algaissi et al., 2018; Hashem et al., 2019; Tao et al., 2015) in Vero-E6 cells. We performed 1:10 serial dilutions of the virus samples using 50 μL as the starting titer until the theoretical dilution was equal to 1 $TCID_{50}$/mL (*i.e.*, 0 log $TCID_{50}$/mL); because the highest viral stock titer was 1×10^7 $TCID_{50}$/mL, of which we used only 100 μL to reach a theoretical maximum titer of 1×10^6 $TCID_{50}$/mL, we performed serial dilutions from 10^{-1} to 10^{-6}. We then aliquoted 100 μL from each dilution to a well on a 96-well microtiter plate of fully confluent Vero-E6 cells, with four wells per dilution and four samples per plate. We incubated the plates infected with the virus at 37 °C for three days, after which we observed each plate for cytopathic effects (CPE) and counted the number of "dead" wells showing CPE in each dilution for each sample. Finally, we estimated the number of viable virus particles using the Reed and Muench method for $TCID_{50}$ quantification (Reed and Muench, 1938).

Each of the four time points at each temperature was performed in triplicate for a total of twelve samples for each temperature, and forty-eight samples in total across all temperatures. We used a 500 μL vial of the virus stock held at room temperature as a positive control and starting titer quantification, denoted by the virus titer at 0 min in Fig. 1B. For the room temperature series of experiments, we immediately titrated the 500 μL virus stock vial as the positive control and starting titer.

2.2. Cells, media, and viruses

The Vero-E6 cells (CRL-1580, American Type Culture Collection) were grown in Eagle's Minimal Essential Medium (MEM) (Corning, 10–010–CV) supplemented with 10% fetal bovine serum (FBS) (GIBCO, 10437–028), 2% L-Glutamine (GIBCO, 25030–164), and 1% Penicillin-Streptomycin (GIBCO, 15140–122), designated 10-MEM. A cell culture medium with a similar composition to 10-MEM, but supplemented with 2% FBS instead of 10% FBS, was designated as 2-MEM and used to culture and transfer the virus. The 2-MEM virus culture medium represents a realistic surrogate for human saliva, through which SARS-CoV-2 is primarily transmitted in the form of aerosolized droplets, in terms of protein concentration, and in fact contains a higher protein concentration (at least 2% total protein per milliliter of medium) than saliva, which has been estimated to contain about 0.3% total protein in a typical 1–2 mL sample (Lagerlof and Dawes, 1984; Schipper et al., 2007; Woo et al., 2010).

The USA-WA1/2020 strain of SARS-CoV-2, provided to us by Dr. Natalie Thornburg at the Centers for Disease Control (CDC), Atlanta, GA, through the World Reference Center for Emerging Viruses and Arboviruses (WRCEVA), was used throughout this study. The original stock of SARS-CoV-2 was cultured in 2-MEM and passaged two more times in Vero-E6 cells to generate the working viral stocks, which were stored at − 80 °C. The two working viral stocks used throughout this study were titrated at either 1×10^5 $TCID_{50}$/mL or 1×10^7 $TCID_{50}$/mL by the standard $TCID_{50}$ assay in Vero-E6 cells as previously described (Algaissi et al., 2018; Hashem et al., 2019; Tao et al., 2015), designated as the "low-titer" and "high-titer" stocks, respectively. Both of these experimental inoculating titers are greater than the average amount of SARS-CoV-2 virions detected in saliva of COVID-19 patients as quantified using quantitative reverse-transcriptase polymerase chain reaction (qRT-PCR), which does not discriminate between replicative and non-replicative viral particles (Ceron et al., 2020). All experiments involving infectious SARS-CoV-2 were conducted at Galveston National Laboratory (GNL) in the biosafety cabinet (BSC) in an approved biosafety level (BSL) laboratory (*i.e.*, BSL-3) following all approved notification-of-use and safety protocols.

2.3. Physical morphology and chemical composition of surgical masks after heating

We visualized the physical structure of the meltblown filter layer (*i.e.*, the middle layer of a typical three-layer surgical mask responsible for filtration) before and after heat treatment at 70 °C for 30 min, 125 °C for 30 min, 150 °C for 10 min, 155 °C for 2 min, and 160 °C for 2 min using scanning electron microscopy. The filter layer was first sputtered

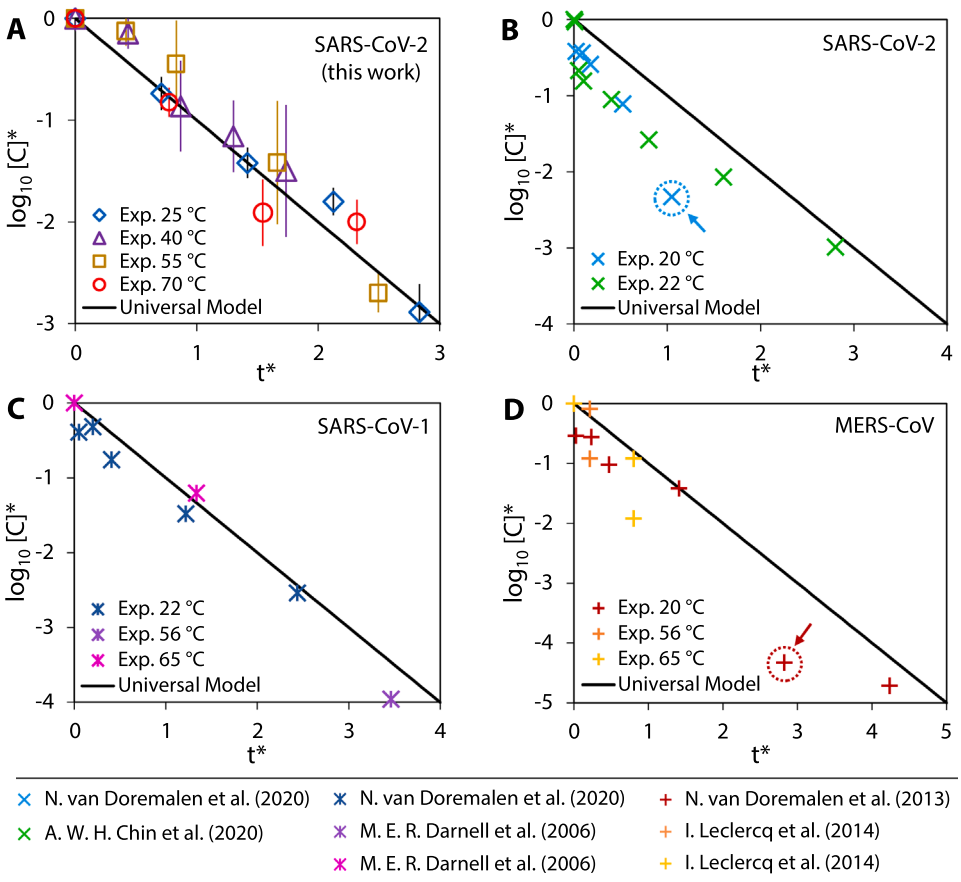

Fig. 2. Self-similar behavior of virus inactivation. The nondimensionalized experimental data for thermal inactivation of SARS-CoV-2 in this work collapse onto a single universal model curve (A). Experimental data from prior work on the thermal inactivation of SARS-CoV-2 (B), SARS-CoV-1 (C), and MERS-CoV (D) were nondimensionalized and compared to our universal model. The comparison reveals that the thermal inactivation processes of all the coronaviruses considered here exhibit the same form of self-similar behavior.

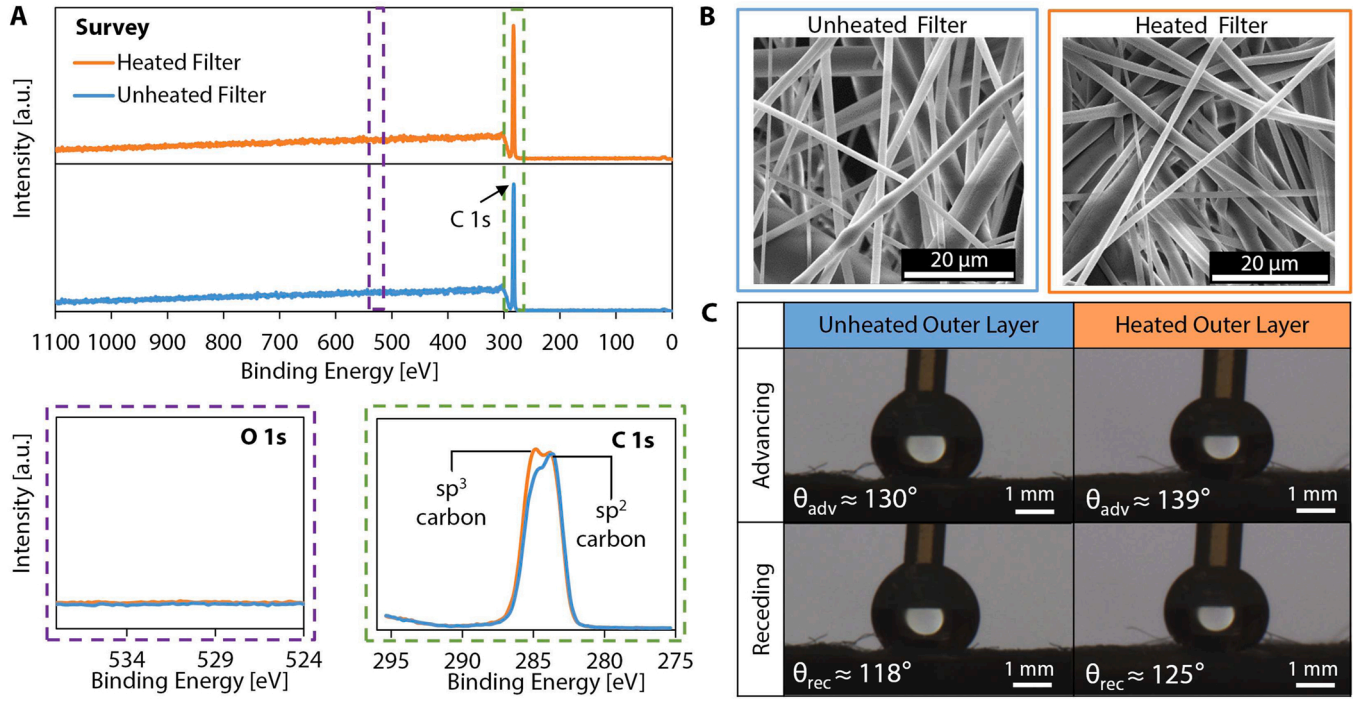

Fig. 3. Chemical composition and physical morphology of a surgical mask before and after heat treatment. The chemical morphology of the disposable mask before and after heat treatment was observed. (A) Survey XPS spectra and detailed O 1s and C 1s spectra were obtained for both the unheated and heated mask filter layers (all vertical scalings are identical). The survey spectra show the same elemental composition for unheated and heated mask filter layers. No oxidation is observed after heat treatment, as evidenced by the detailed O 1s spectra. The detailed C 1s spectra indicate that some sp^2 carbon was converted to sp^3 carbon during heating. (B) Scanning electron microscope (SEM) images show the physical morphology of the meltblown filter layer before and after application of heat treatment at 70 °C for a period of 30 min. (C) Representative images of a droplet advancing and receding on the hydrophobic outer layer of the 3-ply disposable mask and the average contact angle measurements before and after heat treatment at 70 °C for 30 min.

with a 10-nm-thick coating of Au to improve the conductivity of the surface. A field emission scanning electron microscope (FEI Quanta 400 ESEM FEG) was then used to take images with the secondary electron detector at an accelerating voltage of 10 kV.

The chemical composition of the meltblown filter layer before and after heat treatment was characterized using X-ray photoelectron spectroscopy (XPS). The XPS measurements were carried out using a conventional Al Kα (1486.6 eV) X-ray source. A survey scan was conducted to determine the elements present on the surface and detailed scans show the relative peak magnitudes of carbon and oxygen.

We characterized the wettability of the surgical mask hydrophobic outer layer before and after heating with a contact angle goniometer using the sessile drop technique. The advancing and receding water contact angles were measured at 10 different locations on the surgical mask. The goniometer utilized a 5.0 MP, 35 FPS camera (CM3–U3–50S5C–CS Chameleon3, FLIR) equipped with a 0.25x telecentric lens (55–349 GoldTL, Edmund Optics), and the liquid droplet was generated with syringe pump (PHD 2000, Harvard Apparatus) using deionized water at room temperature and pressure. The values of the advancing and receding contact angles were determined by processing the captured images with custom-made Matlab scripts (using polynomial curve fitting to characterize the droplet profile and solid surface).

3. Results and discussion

3.1. Experimental validation of the reaction kinetics model

We conducted dry heat decontamination experiments on surgical masks inoculated with SARS-CoV-2 virus culture at the temperatures and durations shown in Fig. 1B and at a relative humidity (RH) within the range of 48 – 55% at room temperature. As the temperature for a fixed volume of air in the oven increases, the RH inside the oven decreases. Based on the initial vapor density corresponding to a RH of 50% at room temperature (25 °C), we estimate RH values of 23%, 11%, and 6% at 40 °C, 55 °C, and 70 °C, respectively (the steps to determine RH at elevated temperature are included in the Supplementary Material). Our experimental results and model indicate that 70 °C is sufficient to decontaminate surgical masks in less than 5 min according to the FDA-specified 3-log reduction in viable virions (CDC, 2008; FDA, 2020; Oral et al., 2020). We applied our experimental results to validate a model of the reaction kinetics based on the rate law for a first-order reaction and the Arrhenius equation (Yap et al., 2020). This model (Eq. 1) describes the inactivation reaction as thermal degradation of the proteins that comprise each virion (Qiao and De La Cruz, 2020) to predict the time required to achieve an n-log reduction (*i.e.*, the ratio of final viable concentration of virus to its initial concentration in terms of order of magnitude, where $[C]/[C_0] = 10^{-n}$).

$$t_{n-\log} = -\frac{1}{A} e^{\frac{E_a}{RT}} \ln(10^{-n}) \quad \text{(Eq. 1)}$$

The activation energy, E_a, and natural log of the frequency factor, $\ln(A)$, were determined for SARS-CoV-2 on the surgical masks tested in this work using a linear regression approach described in prior work (Yap et al., 2020) and detailed in the Supplementary Material.

The inactivation behavior of SARS-CoV-2 agrees with the Meyer-Neldel rule for entropy-enthalpy compensation exhibited by other coronaviruses (Fig. S3). Furthermore, the E_a and $\ln(A)$ values for SARS-CoV-2 determined in this work deviate by only 2.5% and 1.5%, respectively, from the values determined in prior work based on a data-driven analysis (*i.e.*, without original experimental results) across a range of fomites (Table S6).

This universal model Eq. 1 is plotted in Fig. 1B for the four temperatures studied in this work; the close agreement with the experimental data serves to validate the modeling framework. The data shown here also agree with prior experimental results for room temperature inactivation of SARS-CoV-2 on surgical masks, for which a 3-log reduction requires approximately 100 h (Chin et al., 2020). From experimental results obtained over 25–70 °C, the decontamination time of SARS-CoV-2 on surgical face masks ranges from up to 100 h to as little as 5 min, spanning more than three orders of magnitude and highlighting the exponential dependence of virus inactivation time on temperature as shown in Eq. 1. We note that earlier reports have suggested the possibility of multiple inactivation reaction pathways at different temperatures (Laude, 1981); the data shown here follow a single first-order reaction pathway.

3.2. Self-similarity of virus thermal inactivation

We went on to show that the thermal inactivation process exhibits self-similarity. Self-similar behavior has been identified in phenomena ranging from fluid flows (Aagesen et al., 2010; Day et al., 1998) to complex networks (Ganan-Calvo and Hernandez Ramos, 2020; Song and Havlin, 2005) in prior work, but had not yet been reported for viruses.

To nondimensionalize the relevant parameters, we first define a thermal decontamination timescale, τ_{decon}, in Eq. 2:

$$\tau_{decon} = \frac{\ln(10)}{A} e^{\frac{E_a}{RT}} \quad \text{(Eq. 2)}$$

Nondimensionalizing time with respect to the thermal decontamination timescale yields the dimensionless time, $t^* = t/\tau_{decon}$. The concentration is then nondimensionalized by dividing by the initial concentration, $[C]^* = [C]/[C_0]$.

Plotting the nondimensionalized experimental data, we show that the data points collapse onto a single universal model prediction (Fig. 2A) for which $n = -t^*$, indicating that the thermal inactivation process exhibits fundamental self-similarity and the order of viral reduction, n, is directly proportional to t^*. This new understanding will allow application of our results across a wide range of temperatures beyond the four specific temperatures studied here.

From the nondimensionalized plot, we are also able to identify the experimental temperature and duration that achieves a desired n-log reduction. We compared our universal model prediction to prior experimental work on SARS-CoV-2 (Chin et al., 2020; van Doremalen et al., 2020), SARS-CoV-1 (Darnell and Taylor, 2006; van Doremalen et al., 2020), and MERS-CoV (Leclercq et al., 2014; van Doremalen et al., 2013) and found that, upon nondimensionalizing the data from these reports, the inactivation trend was also described by our model and exhibited self-similarity (Fig. 2B – D). These three coronaviruses were chosen because they are highly pathogenic human coronaviruses and the results could be relevant to further understand their inactivation behavior (Cevik et al., 2021; Zhu et al., 2020). The inactivation results reported in literature for these three coronaviruses generally follow the self-similar trend with the exception of two outliers indicated with arrows in Fig. 2B and D; outliers were determined using a standard procedure based on the standard deviation of the residuals (Illowsky and Dean, 2021). The deviation of these two outliers from the universal model prediction may indicate potential experimental error in the results, suggesting that researchers working on the thermal inactivation of viruses can use this model as a benchmark to compare against experiments in future work.

3.3. Surgical masks before and after dry heat decontamination

To complement the underlying concept of thermal inactivation of viruses and enable practical use, prior work has focused on studying the filtration performance and fit test of disposable masks after dry heat decontamination. Oh et al. performed filtration performance, pressure drop, and quantitative fit testing after dry heat decontamination at 100 °C and 5% RH for 50 min. After 20 cycles of decontamination, they found that the particle filtration efficiency was 97% (above the minimum filtration efficiency requirement of 95% for N95 respirators), with no significant changes in pressure drop (Oh et al., 2020). The average fit factor was 139, well above the passing score of 100. Another study by Xiang et al. conducted dry heat decontamination of N95 respirators and surgical masks at 70 °C for 1, 2, and 3 h and showed that filtration efficiencies remained greater than 96% (Xiang et al., 2020). Additional

work studying the electrostatic charge on mask filter layers, which is partially responsible for filtering of small particles by electrostatic adsorption, found that dry heat treatment at low humidities (< 30% RH) and low temperatures (< 100 °C) for 20 cycles did not decay the electrostatic charges and the efficiency of the filters (Campos et al., 2020; Liao et al., 2020). Fit tests conducted by Zha et al. after one cycle of dry heat decontamination at 75 °C for 30 min show that 93% of N95 respirators passed the fit test if the respirator was donned and doffed less than 5 times prior to dry heat decontamination (Zha et al., 2021).

The results presented in the literature indicate that dry heat decontamination at 70 °C (the maximum temperature applied in this work) for 5 min will not degrade the filtration efficiency of masks; to further supplement prior results, we provide additional characterization of the effect of dry heat treatment on the material properties of the mask layers at 70 °C for 30 min (more than six times the duration required for effective decontamination) to yield fundamental insight into the micro- and nanoscale morphology and chemical composition of disposable masks and N95 respirators (*i.e.,* masks made from nonwoven polypropylene fibers). We characterized the chemical composition of the meltblown filter layer (*i.e.*, the middle layer of a typical three-layer surgical mask responsible for filtration) using X-ray photoelectron spectroscopy (XPS). The XPS survey spectrum as well as detailed O 1s and C 1s spectra of the unheated and heated filters are shown in Fig. 3A. Heat treatment at 70 °C for 30 min did not alter the elemental composition, nor did it result in any oxidation as evidenced by the detailed O 1s spectra. The detailed C 1s spectra indicate that some sp^2 carbon converted to sp^3 during the heating process, which suggests strengthening of the material in an annealing-like process and a potential increase in surface hydrophobicity (Paul et al., 2008).

We visualized the physical morphology of the meltblown filter layer of the surgical mask before and after heat treatment using electron microscopy (Fig. 3B). The images in Fig. 3B show that there are no apparent physical changes in the microscale morphology or structure of the fibers. In contrast, we also heated surgical masks to high temperatures typical for dry heat decontamination (~160 °C) and observed significant degradation of the meltblown filter layer (Fig. S5), illustrating the sensitivity of the material properties and physical morphology of the meltblown filter layer to temperature, especially when operating close to the melting point of the polymer.

To ensure that the functionality of the hydrophobic outer layer of the 3-ply surgical mask (*i.e.*, the outermost layer relative to the wearer) was not altered after dry heat decontamination, water contact angle measurements were taken on the outer layer before and after heat treatment at 70 °C for 30 min; we found that the heat treatment did not significantly change the surface wettability of the hydrophobic mask layer (Fig. 3C). We observed small increases in the advancing and receding contact angles (average values shown in Fig. 3C) on the outer layer after heat treatment, likely due to the conversion of sp^2 carbon to sp^3 carbon during the heating process as observed on the meltblown filter layer. These results indicate that dry heat decontamination, in addition to effectively inactivating SARS-CoV-2 in short times and at temperatures available in most home devices, is also appropriate for delicate PPE, including masks.

3.4. Limitations of the universal model

We note that the model presented here focuses solely on the effect of temperature and does not consider relative humidity, which has been shown to affect virus lifetime (Chan et al., 2011; Lin and Marr, 2020); however, recent work suggests that relative humidity may be integrated into a reaction-rate-based model, such as the one presented in this work (Morris et al., 2020). Different fomites are also known to alter virus lifetime by up to an order of magnitude (Bayarri et al., 2021; Imani et al., 2020; van Doremalen et al., 2020), and incorporation of fomite material in the model, interpreted as a catalyst (*i.e.*, by modifying E_a and $\ln(A)$), may allow this modeling framework to accurately predict virus lifetimes across a range of fomites (Roduner, 2014). We also note that the salt and protein concentrations in the virus culture medium could affect the virus' resistance to heat; in future work, we could use our current work as a baseline to study the effects of salt and protein concentration on the temperature-dependent rate of inactivation. The model is limited in terms of extrapolation to higher temperatures, for which alternate reaction pathways may dominate. Finally, we note that the samples were assumed to have a constant temperature during decontamination due to the short transient heating periods (at most, ~10% of the total heating duration for the shortest decontamination duration at 70 °C as detailed in the Supplementary Material); however, time-varying temperature profiles could be accounted for by adjusting the model for objects with a larger thermal mass that exhibit longer time-dependent temperatures as they equilibrate with their surroundings (Yap et al., 2021).

4. Conclusions

This work validates a model based on reaction kinetics to predict the time required for SARS-CoV-2 decontamination, providing much-needed guidelines to allow safe reuse of PPE. With this modeling framework, the number of experiments required to characterize the effects of temperature for a specific virus can be greatly reduced, and early dissemination of decontamination guidelines for yet-unencountered novel viruses will become attainable. In addition to temperature, the decontamination timescale is a function of the activation energy and the frequency factor; adjusting E_a and $\ln(A)$ would allow for the thermal inactivation behavior of most viruses to collapse onto the single unified model curve presented in this work. Extension of the model to include environmental conditions such as relative humidity and fomite material could ultimately provide a pathway toward a comprehensive model of virus inactivation that applies to all viruses, with the self-similar behavior of the thermal inactivation process applied as a metric to understand the requirements for safe and effective decontamination.

CRediT authorship contribution statement

Te Faye Yap: Conceptualization, Formal analysis, Visualization, Methodology, Writing – original draft, Writing – review & editing. **Jason Hsu:** Investigation, Methodology, Writing – review & editing. **Zhen Liu:** Methodology, Visualization, Writing – review & editing. **Kempaiah Rayavara:** Investigation, Writing – review & editing. **Vivian Tat:** Investigation, Writing – review & editing. **Chien-Te K. Tseng:** Supervision, Funding acquisition, Writing – review & editing. **Daniel J. Preston:** Supervision, Conceptualization, Methodology, Funding acquisition, Writing – original draft, Writing – review & editing.

Declaration of Competing Interest

The authors declare that they have no known competing financial interests or personal relationships that could have appeared to influence the work reported in this paper.

Acknowledgments

This work was supported by the National Science Foundation under grants CBET-2030023 and CBET-2030117 with Dr. Ying Sun as program director. This work was conducted in part using resources provided by the Shared Equipment Authority at Rice University. We would like to acknowledge Dr. Aleksandra Drelich for technical assistance provided in interpreting preliminary results and constructive suggestions during the planning of this project.

Appendix A. Supporting information

Supplementary data associated with this article can be found in the online version at doi:10.1016/j.jhazmat.2021.127709.

References

Aagesen, L.K., Johnson, A.E., Fife, J.L., Voorhees, P.W., Miksis, M.J., Poulsen, S.O., Lauridsen, E.M., Marone, F., Stampanoni, M., 2010. Universality and self-similarity in pinch-off of rods by bulk diffusion. Nat. Phys. 6, 796–800. https://doi.org/10.1038/nphys1737.

Algaissi, A., Agrawal, A.S., Han, S., Peng, B.-H., Luo, C., Li, F., Chan, T.-S., Couch, R.B., Tseng, C.-T.K., 2018. Elevated human dipeptidyl peptidase 4 expression reduces the susceptibility of hDPP4 transgenic mice to middle east respiratory syndrome coronavirus infection and disease. J. Infect. Dis. 219, 829–835. https://doi.org/10.1093/infdis/jiy574.

Bayarri, B., Cruz-Alcalde, A., López-Vinent, N., Micó, M.M., Sans, C., 2021. Can ozone inactivate SARS-CoV-2? A review of mechanisms and performance on viruses. J. Hazard. Mater. 415. https://doi.org/10.1016/j.jhazmat.2021.125658.

Callaway, E., 2021. Delta coronavirus variant: scientists brace for impact. Nature 595, 17–18. https://doi.org/10.1038/d41586-021-01696-3.

Campos, R.K., Jin, J., Rafael, G.H., Zhao, M., Liao, L., Simmons, G., Chu, S., Weaver, S.C., Chiu, W., Cui, Y., 2020. Decontamination of SARS-CoV-2 and other RNA viruses from N95 level meltblown polypropylene fabric using heat under different humidities. ACS Nano 14, 14017–14025. https://doi.org/10.1021/acsnano.0c06565.

CDC, 2008. Disinfection of Healthcare Equipment. ⟨https://www.cdc.gov/infectioncontrol/guidelines/disinfection/healthcare-equipment.html⟩.

Ceron, J.J., Lamy, E., Martinez-Subiela, S., Lopez-Jornet, P., Silva, Capela E., Eckersall, F., Tvarijonaviciute, A, P.D., 2020. Use of saliva for diagnosis and monitoring the SARS-CoV-2: a general perspective. J. Clin. Med. 9, 1491. https://doi.org/10.3390/jcm9051491.

Cevik, M., Tate, M., Lloyd, O., Maraolo, A.E., Schafers, J., Ho, A., 2021. SARS-CoV-2, SARS-CoV, and MERS-CoV viral load dynamics, duration of viral shedding, and infectiousness: a systematic review and meta-analysis. Lancet Microbe 2, e13–e22. https://doi.org/10.1016/S2666-5247(20)30172-5.

Chan, K.H., Peiris, J.S.M., Lam, S.Y., Poon, L.L.M., Yuen, K.Y., Seto, W.H., 2011. The effects of temperature and relative humidity on the viability of the SARS coronavirus. Adv. Virol. 2011, 1–7. https://doi.org/10.1155/2011/734690.

Chin, A.W.H., Chu, J.T.S., Perera, M.R.A., Hui, K.P.Y., Yen, H.-L., Chan, M.C.W., Peiris, M., Poon, L.L.M., 2020. Stability of SARS-CoV-2 in different environmental conditions. Lancet Microbe 1, e10. https://doi.org/10.1016/S2666-5247(20)30003-3.

Cramer, A., Tian, E., Yu, S.H., Galanek, M., Lamere, E., Li, J., Gupta, R., Short, M.P., 2020. Disposable N95 masks pass qualitative fit-test but have decreased filtration efficiency after cobalt-60 gamma irradiation. medRxiv. https://doi.org/10.1101/2020.03.28.20043471.

Darnell, M.E.R., Taylor, D.R., 2006. Evaluation of inactivation methods for severe acute respiratory syndrome coronavirus in noncellular blood products. Transfusion 46, 1770–1777. https://doi.org/10.1111/j.1537-2995.2006.00976.x.

Day, R.F., Hinch, E.J., Lister, J.R., 1998. Self-similar capillary pinchoff of an inviscid fluid. Phys. Rev. Lett. 80, 704–707. https://doi.org/10.1103/PhysRevLett.80.704.

FDA, 2020. Investigating Decontamination and Reuse of Respirators in Public Health Emergencies.

Ganan-Calvo, A.M., Hernandez Ramos, J.A., 2020. The fractal time growth of COVID-19 pandemic: an accurate self-similar model, and urgent conclusions. arXiv 1–13.

Hashem, A.M., Algaissi, A., Agrawal, A.S., Al-Amri, S.S., Alhabbab, R.Y., Sohrab, S.S., Almasoud, S., Alharbi, A., Peng, N.K., Russell, B.-H., Li, M., Tseng, C.-T.K, X., 2019. A highly immunogenic, protective, and safe adenovirus-based vaccine expressing middle east respiratory syndrome coronavirus S1-CD40L fusion protein in a transgenic human dipeptidyl peptidase 4 mouse model. J. Infect. Dis. 220, 1558–1567. https://doi.org/10.1093/infdis/jiz137.

Iijima, Y., Karama, M., Oundo, J.O., Honda, T., 2001. Prevention of bacterial diarrhea by pasteurization of drinking water in Kenya. Microbiol. Immunol. 45, 413–416. https://doi.org/10.1111/j.1348-0421.2001.tb02639.x.

Illowsky, B., Dean, S., 2021. Outliers. https://stats.libretexts.org/@go/page/802 (accessed 10.7.21).

Imani, S.M., Ladouceur, L., Marshall, T., Maclachlan, R., Soleymani, L., Didar, T.F., 2020. Antimicrobial nanomaterials and coatings: current mechanisms and future perspectives to control the spread of viruses including SARS-CoV-2. ACS Nano 14, 12341–12369. https://doi.org/10.1021/acsnano.0c05937.

Islam, M.F., Johnston, R.B., 2006. Household pasteurization of drinking-water: the Chulli water-treatment system. J. Health Popul. Nutr. 24, 356–362. https://doi.org/10.3329/jhpn.v24i3.721.

Jinia, A.J., Sunbul, N.B., Meert, C.A., Miller, C.A., Clarke, S.D., Kearfott, K.J., Matuszak, M.M., Matuszak, M.M., Pozzi, S.A., 2020. Review of sterilization techniques for medical and personal protective equipment contaminated with SARS-CoV-2. IEEE Access 8, 111347–111354. https://doi.org/10.1109/ACCESS.2020.3002886.

Kolata, G., 2020. As Coronavirus Looms, Mask Shortage Gives Rise to Promising Approach. New York Times.

Lagerlof, F., Dawes, C., 1984. The volume of saliva in the mouth before and after swallowing. J. Dent. Res. 63, 618–621. https://doi.org/10.1177/00220345840630050201.

Laude, H., 1981. Thermal inactivation studies of a coronavirus, transmissible gastroenteritis virus. J. Gen. Virol. 56. https://doi.org/10.1099/0022-1317-56-2-235.

Leclercq, I., Batéjat, C., Burguière, A.M., Manuguerra, J.C., 2014. Heat inactivation of the Middle East respiratory syndrome coronavirus. Influenza Other Respi. Viruses. https://doi.org/10.1111/irv.12261.

Liao, D.L., Xiao, W., Yu, X., Wang, H., Zhao, D.M., Wang, D.Q., 2020. Can N95 facial masks be used after disinfection? And for how many times? ACS Nano 14, 6348–6356. https://doi.org/10.1021/acsnano.0c03597.

Lin, K., Marr, L.C., 2020. Humidity-dependent decay of viruses, but not bacteria, in aerosols and droplets follows disinfection kinetics. Environ. Sci. Technol. 54, 1024–1032. https://doi.org/10.1021/acs.est.9b04959.

Mahase, E., 2021. Delta variant: what is happening with transmission, hospital admissions, and restrictions? BMJ 373, 1–2. https://doi.org/10.1136/bmj.n1513.

Morris, D.H., Claude Yinda, K., Gamble, A., Rossine, F.W., Bushmaker, T., Fischer, R.J., Jeremiah Matson, M., van Doremalen, N., Vikesland, P.J., Marr, L.C., Munster, V.J., Lloyd-Smith, J.O., 2020. Mechanistic theory predicts the effects of temperature and humidity on inactivation of SARS-CoV-2 and other enveloped viruses. bioRxiv. https://doi.org/10.1101/2020.10.16.341883.

Oh, C., Araud, E., Puthussery, J.V., Bai, H., Clark, G.G., Wang, L., Verma, V., Nguyen, T. H., 2020. Dry heat as a decontamination method for n95 respirator reuse. Environ. Sci. Technol. Lett. 7, 677–682. https://doi.org/10.1021/acs.estlett.0c00534.

Oral, E., Wannomae, K.K., Connolly, R., Gardecki, J., Leung, H.M., Muratoglu, O., Griffiths, A., Honko, A.N., Avena, L.E., Mckay, L.G.A., Flynn, N., Storm, N., Downs, S.N., Jones, R., Emmal, B., 2020. Vapor H 2 O 2 sterilization as a decontamination method for the reuse of N95 respirators in the COVID-19 emergency 4, 1–5. https://doi.org/10.1101/2020.04.11.20062026.

Paul, R., Das, S.N., Dalui, S., Gayen, R.N., Roy, R.K., Bhar, R., Pal, A.K., 2008. Synthesis of DLC films with different sp2/sp3 ratios and their hydrophobic behaviour. J. Phys. D Appl. Phys. 41. https://doi.org/10.1088/0022-3727/41/5/055309.

Qiao, B., De La Cruz, M.O., 2020. Enhanced binding of SARS-CoV-2 spike protein to receptor by distal polybasic cleavage sites. ACS Nano 14, 10616–10623. https://doi.org/10.1021/acsnano.0c04798.

Raeiszadeh, M., Adeli, B., 2020. A critical review on ultraviolet disinfection systems against COVID-19 outbreak: applicability, validation, and safety considerations. ACS Photonics 7, 2941–2951. https://doi.org/10.1021/acsphotonics.0c01245.

Reed, L.J., Muench, H., 1938. A simple method of estimating fifty per cent endpoints. Am. J. Epidemiol. 27, 493–497. https://doi.org/10.1093/oxfordjournals.aje.a118408.

Roduner, E., 2014. Understanding catalysis. Chem. Soc. Rev. 43, 8226–8239. https://doi.org/10.1039/c4cs00210e.

Rowan, N.J., Laffey, J.G., 2020. Challenges and solutions for addressing critical shortage of supply chain for personal and protective equipment (PPE) arising from Coronavirus disease (COVID19) pandemic – case study from the Republic of Ireland. Sci. Total Environ. 725, 138532 https://doi.org/10.1016/j.scitotenv.2020.138532.

Samarasekera, U., 2021. India grapples with second wave of COVID-19. Lancet Microbe 2, e238. https://doi.org/10.1016/s2666-5247(21)00123-3.

Sanche, S., Lin, Y.T., Xu, C., Romero-Severson, E., Hengartner, N., Ke, R., 2020. High contagiousness and rapid spread of severe acute respiratory syndrome coronavirus 2. Emerg. Infect. Dis. 26, 1470–1477. https://doi.org/10.3201/eid2607.200282.

Schipper, R.G., Silletti, E., Vingerhoeds, M.H., 2007. Saliva as research material: biochemical, physicochemical and practical aspects. Arch. Oral. Biol. 52, 1114–1135. https://doi.org/10.1016/j.archoralbio.2007.06.009.

Song, C., Havlin, S., 2005. Self-similarity of complex networks. Nature 433, 392–395. https://doi.org/10.1038/nature03248.

Tao, X., Garron, T., Agrawal, A.S., Algaissi, A., Peng, B.-H., Wakamiya, M., Chan, T.-S., Lu, L., Du, L., Jiang, S., Couch, R.B., Tseng, C.-T.K., 2015. Characterization and demonstration of the value of a lethal mouse model of middle east respiratory syndrome coronavirus infection and disease. J. Virol. 90, 57–67. https://doi.org/10.1128/JVI.02009-15.

van Doremalen, N., Bushmaker, T., Morris, D.H., Holbrook, M.G., Gamble, A., Williamson, B.N., Tamin, A., Harcourt, J.L., Thornburg, N.J., Gerber, S.I., Lloyd-Smith, J.O., de Wit, E., Munster, V.J., 2020. Aerosol and surface stability of SARS-CoV-2 as compared with SARS-CoV-1. N. Engl. J. Med. 382, 1564–1567. https://doi.org/10.1056/NEJMc2004973.

van Doremalen, N., Bushmaker, T., Munster, V.J., 2013. Stability of middle east respiratory syndrome coronavirus (MERS-CoV) under different environmental conditions. Eurosurveillance 18, 1–4. https://doi.org/10.2807/1560-7917.ES2013.18.38.20590.

Viscusi, D.J., Bergman, M.S., Eimer, B.C., Shaffer, R.E., 2009. Evaluation of five decontamination methods for filtering facepiece respirators. Ann. Occup. Hyg. 53, 815–827. https://doi.org/10.1093/annhyg/mep070.

Viscusi, D.J., King, W.P., Shaffer, R.E., 2007. Effect of decontamination on the filtration efficiency of two filtering facepiece respirator models. J. Int. Soc. Respir. Prot. 24.

Woo, M.-H., Hsu, Y.-M., Wu, C.-Y., Heimbuch, B., Wander, J., 2010. Method for contamination of filtering facepiece respirators by deposition of MS2 viral aerosols. J. Aerosol Sci. 41, 944–952. https://doi.org/10.1016/j.jaerosci.2010.07.003.

Xiang, Y., Song, Q., Gu, W., 2020. Decontamination of surgical face masks and N95 respirators by dry heat pasteurization for one hour at 70°C. Am. J. Infect. Control 48, 880–882. https://doi.org/10.1016/j.ajic.2020.05.026.

Yap, T.F., Decker, C.J., Preston, D.J., 2021. Effect of daily temperature fluctuations on virus lifetime. Sci. Total Environ. 789, 148004 https://doi.org/10.1016/j.scitotenv.2021.148004.

Yap, T.F., Liu, Z., Shveda, R.A., Preston, D.J., 2020. A predictive model of the temperature-dependent inactivation of coronaviruses. Appl. Phys. Lett. 117. https://doi.org/10.1063/5.0020782.

Zha, M., Alsarraj, J., Bunch, B., Venzon, D., 2021. Impact on the fitness of N95 masks with extended use/limited reuse and dry heat decontamination. J. Investig. Med. https://doi.org/10.1136/jim-2021-001908.

Zhu, Y., Chen, Y.Q., 2020. On a statistical transmission model in analysis of the early phase of COVID-19 outbreak. Stat. Biosci. 13, 1–17. https://doi.org/10.1007/s12561-020-09277-0.

Zhu, Z., Lian, X., Su, X., Wu, W., Marraro, G.A., Zeng, Y., 2020. From SARS and MERS to COVID-19: a brief summary and comparison of severe acute respiratory infections caused by three highly pathogenic human coronaviruses. Respir. Res. 21, 1–14. https://doi.org/10.1186/s12931-020-01479-w.